Journal of Engineering Mathematics **42:** 203–221, 2002.

On collocation schemes for integral equations arising in slender-body approximations of flow past particles with circular cross-section

THOMAS GÖTZ
Department of Mathematics, University of Kaiserslautern, D-67663 Kaiserslautern, Germany
(e-mail: goetz@mathematik.uni-kl.de)

Received 1 November 2000; accepted in revised form 15 February 2002

Abstract. A collocation method is presented for solving a singular integral equation of the second kind arsing in the slender-body approximation of viscous flow past slender bodies. When the spectral representation of the integral operator is explicitly known, the collocation method is shown to recover the spectrum of the continuous operator. The approximation error is estimated for two discretizations of the integral operator, and convergence is proved. The collocation scheme is validated for several test cases and extended to situations where the spectrum is not explicitly known.

Key words: collocation method, slender-body approximation, singular integral equation.

1. Introduction

Artificial fibers such as Nylon are typically produced by the so-called wet-spinning [1] or melt-spinning [2–5] process. In the melt-spinning process, the molten polymer granulate is pressed through an array of circular nozzles called the spinneret, and the polymer jet produced by each nozzle enters a vertical cooling chamber and solidifies. To speed up the cooling process, a light air stream with a velocity less than 1 m/s is blown against the fibers. At the end of the cooling chamber (after approximately 3 to 5 m), the finished fibers are wound up by spindles. Simulation of the fiber formation and fiber-air interaction is an important tool for increasing the production rate and monitoring quality. Since the fibers have curved shapes and a varying radius along their longitudinal coordinate, the calculation of the force that the exterior flow with Reynolds number based on fiber radius $\approx 0{\cdot}1$ to 1 exerts on such a slender object with length-to-radius ratio $\approx 10^5$–10^6 is both an important and non-trivial task. Similar problems arise in rheological investigations of fiber-reinforced materials [6–8] where slender glass-fibers (length-to-radius ratio $\approx 10^3$) are embedded in a polymer. To simulate the flow of such a composite material, one needs to understand the motion of the glass fibers in the surrounding polymer, and estimate the forces exerted onto them. Phase transitions of liquid crystals [9] lead to similar problems. The interaction of tissues fibers with a blood stream [10] and animal locomotion [11] are additional examples drawn from the field of biofluiddynamics.

In these technological and biological processes, it is important to understand the interaction of long, slender and curved fibers with the surrounding fluid. The numerical calculation of the forces acting on a fiber is a key point in the simulations. Asymptotically, the force acting on a slender particle can be described by an integral equation [12]. In [13,14], exact solutions were provided for some test cases. In [5,15], the spectral properties of the underlying integral opera-

tor were investigated. However, a numerical treatment of the asymptotic integral equation (1), and of similar integral equations arising in Selliers's approach see [14, Equation (4.11)], is needed. As an alternative to the collocation method presented here, a Galerkin-type method is described in [16].

In Section 2 we briefly describe the integral-equation model for the interaction force density in the case of linearized flow and discuss available theoretical results [5,14,15]. A collocation method for solving the integral equation in the case of a straight fiber is presented in Section 3. The approximation error of this scheme is estimated in Section 3.2, and it is shown to be of second order in the spatial grid size h. In Section 3.3 the scheme is shown to reproduce the spectrum of the operator S. Convergence is proved in Section 3.4. The discretization of the general equation for curved fibers is discussed in Section 4. Comparisons of numerical solutions based on the proposed collocation scheme with spectral methods for test cases considered by other authors are presented in Section 5. Proofs of some identities are presented in the Appendix.

2. An integral equation for the force density acting on a fiber

Asymptotically, a slender fiber immersed in a viscous fluid can be viewed as an one-dimensional object with infinitesimal cross-section. Assuming linearized hydrodynamics, we express the flow field as a superposition of fundamental solutions, so-called Stokeslets [13], placed along the centerline of the fiber. Matching asymptotic expansions and applying the no-slip condition on the fiber surface we obtain a Fredholm integral equation of the second kind for the distribution of the fundamental solutions [5,12] which can be used to determine the force that the fluid exerts onto the fiber.

For a long, slender fiber with circular cross-section exposed to a free-flow, the integral equation for the force density φ acting on the fiber satisfies the equation (Appendix A)

$$8\pi\mu\,(\boldsymbol{u_0}(s)-\boldsymbol{u}_\infty(s)) = \mathbf{C}(s)\boldsymbol{\varphi}(s)+\int_0^1\left(\frac{\boldsymbol{\varphi}(t)}{R_0}-\frac{\boldsymbol{\varphi}(s)}{|s-t|}+\frac{\mathbf{M_0}\boldsymbol{\varphi}(t)}{R_0^3}-\frac{\boldsymbol{e_t}\boldsymbol{e_t}'\boldsymbol{\varphi}(s)}{|s-t|}\right)\mathrm{d}t+\mathcal{O}(a), \tag{1}$$

where $\boldsymbol{u_0}$ is the velocity of the fiber, $\boldsymbol{u}_\infty$ is a free-stream velocity profile, $\mu>0$ is the viscosity of the fluid, and $s\in[0,1]$ is the arc length parameter normalized by the total length of the fiber. The function $\mathbf{C}:[0,1]\to\mathbb{R}^{3\times3}$ is given by $\mathbf{C}(s)=(\mathbf{I}+\boldsymbol{e_t}\boldsymbol{e_t}')+(\mathbf{I}-3\boldsymbol{e_t}\boldsymbol{e_t}')$, where, $\mathbf{I}$ is the identity matrix in $\mathbb{R}^{3\times3}$, $\boldsymbol{e_t}\in\mathbb{R}^3$ is the unit tangent vector to the fiber's centerline (depending on s), and $\boldsymbol{e_t}'$ is its transpose. The function $L(s)=\log\frac{s(1-s)}{4a^2\rho^2(s)}$ depends on the slenderness ratio $a\ll1$ and the local radius $\rho(s)$ of the fiber. The distance between two points $\boldsymbol{x_0}(t)$ and $\boldsymbol{x_0}(s)$ on the centerline $\boldsymbol{x_0}:[0,1]\to\mathbb{R}^3$ is denoted by $R_0=\|\boldsymbol{R}\|_2$, where $\boldsymbol{R_0}=\boldsymbol{x_0}(t)-\boldsymbol{x_0}(s)$. The matrix $\mathbf{M_0}\in\mathbb{R}^{3\times3}$ is defined by $\mathbf{M_0}=\boldsymbol{R_0}\boldsymbol{R_0}'$. Strictly speaking R_0, $\boldsymbol{R_0}$ and $\mathbf{M}_0$ depend on both s and t. However, to simplify the notation, we skip this dependence henceforth. The unknown vector-valued function $\boldsymbol{\varphi}(s)$ is the force per unit length acting on the fiber.

A detailed derivation of the integral equation (1) in the case of Stokes's and Oseen's equation can be found in [5]. Alternatively, Sellier [14] derives the surface stress by solving asymptotically a Fredholm integral equation of the first kind.

The integral equation (1) is valid away from the ends of the body, but the neglected end effects are important only at higher-order approximations [17,18]. In [13, 17, 18] it was argued, that the force distribution $\boldsymbol{\varphi}$ should be defined only on same interior part $[\alpha,\beta]$ with

$0 < \alpha < \beta < 1$ of the centerline. The numerical scheme presented in Section 3 takes this into account, since the collocation points are placed at the mid-points of the grid cells rather than at the end-points.

In particular, if a straight fiber moving with a velocity u_0 is exposed to an uniform free-flow u_∞ normal to it, we obtain the scalar equation

$$(C + S)[\varphi] = f, \quad \text{and} \quad S[\varphi](s) = \int_0^1 \frac{\varphi(t) - \varphi(s)}{|t - s|}\, \mathrm{d}t, \tag{2}$$

where $C(s) = \log(s(1-s)/a^2\rho^2(s)) + 1$ and $f = 8\pi\nu(u_0(s) - u_\infty(s))$ in Equation (1). Considering a fiber with ellipsoidal shape, *i.e.* $\rho(s) = k\sqrt{s(1-s)}$ for some $k > 0$, the function $C(s)$ reduces to a constant $c > 0$ [5,12].

Some of the assumptions made in deriving (1) can be relaxed; we can allow for a non-circular cross-section of the fiber [14, 19–21]. As mentioned in the introduction, in the industrial application of fiber spinning the case of circular cross-sections is especially relevant.

An extension of the theory to Oseen flow and to heat transport around a heated fiber is also possible [5]. Both Oseen's equation (for the flow-field) and the heat-conduction equation including linearized convection, yield similar integral equations.

2.1. Theoretical results for Equation (2)

In [5,15], a complete theory of (2) was developed. The results are based on the knowledge of the spectrum of eigenvalues of the integral operator S :

$$\sigma(S) = \{-L_k : k \in \mathbb{N}_0\}, \tag{3}$$

given by $L_k = \sum_{i=1}^{k} 2/i$ for $k \in \mathbb{N}$ and $L_0 = 0$. The associated eigenfunctions are the Legendre polynomials P_k rescaled to the interval [0,1], $S(P_k) = -L_k P_k$. This knowledge suggests the application of spectral methods to solve (2). In [5,15], conditions for the existence and uniqueness of solutions φ belonging to $\mathcal{L}^2$ as well as $\mathcal{C}^1$ are established.

However, in the general case (1), neither the spectrum nor the eigenfunctions of the integral operator are available, and spectral techniques cannot be applied. Moreover, because the integral operator is unbounded, computing the solution via successive approximations (see for example [12]) is not possible.

The main purpose of the present work is to provide a sound numerical method for solving the integral equation (1). In Section 3, a collocation method for the case corresponding to (2) is proposed, and then extended to the general case in Section 4.

3. Collocation schemes

Following the basic idea of the collocation method, we replace the continuous equation (2) with a finite number of equations $(C+S)[\varphi](\chi) = f(\chi)$ applied at collocation points $\chi \in \mathcal{X}$. Choosing an appropriate space of *ansatz* functions and a suitable numerical quadrature, we can approximate the integral operator S with a matrix $\mathbf{S_0}$, and the multiplication operator C with another matrix $\mathbf{C}$. Solving the resulting system of linear algebraic equations $(\mathbf{C} + \mathbf{S_0})\boldsymbol{\psi} = \boldsymbol{f}$ we obtain an approximation $\boldsymbol{\psi}$ for φ.

3.1. NOTATION

Let $n \in \mathbb{N}$. We define an *equidistant grid* on the interval $[0, 1]$ with a mesh width $h = 1/n$ and grid nodes $s_i = ih$ for $i = 0, \dots, n$. This grid defines the cells $Z_i = [s_{i-1}, s_i)$ for $i = 1, \dots, n-1$ and $Z_n = [s_{n-1}, s_n]$. Their mid-points are denoted by $\chi_i = (i - 1/2)h$ for $i = 1, \dots, n$, and the set of *collocation points* is denoted by $\mathcal{X} = \{\chi_i, i = 1, \dots, n\}$.

Let $I \subset \mathbb{R}$ denote an interval. In the following we will need the function spaces

$$\begin{aligned}
\mathcal{B}(I) &:= \left\{ f : I \mapsto \mathbb{R} : \ \|f\|_\infty := \sup_{x \in I} |f(x)| \leq \infty \right\}, \\
\mathcal{C}^k(I) &:= \{ f : I \mapsto \mathbb{R} : \ f \text{ is } k\text{-times continuously differentiable} \}, \\
\mathcal{P}_n &:= \{ f : I \mapsto \mathbb{R} : \ f \text{ is a polynomial of maximal degree } n \}, \\
\mathcal{P}_n^{\mathrm{pw}} &:= \{ f : I \mapsto \mathbb{R} : \ f|_{Z_i} \in P_n \text{ for all grid cells} Z_i, i = 1, \dots, n \}.
\end{aligned}$$

The *restriction* and an *extension* operator that map functions from the interval $[0, 1]$ onto the collocation points and *vice versa* can now be defined on the appropriate function spaces as follows. Let $\varphi \in \mathcal{B}[0, 1]$. We define the *restriction operator* $R : \mathcal{B}[0, 1] \mapsto \mathbb{R}^n$ by $(R[\varphi])_i := \varphi(\chi_i)$, where $R[\varphi]$ is called the *grid function associated with* φ. For $\boldsymbol{\psi} \in \mathbb{R}^n$, the *piecewise constant extension operator* $E_0 : \mathbb{R}^n \mapsto \mathcal{P}_0^{\mathrm{pw}}$ is defined by $(E_0[: \boldsymbol{\psi}])(s) := \psi_i$ for $s \in Z_i$ and $i = 1, \dots, n$.

Since a grid function can be identified with a vector in $\mathbb{R}^n$, we use the norms

$$\begin{aligned}
\|\boldsymbol{\psi}\|_p &:= \left(\sum_{i=1}^{n} |\psi_i|^p \right)^{1/p}, \quad 1 \leq p < \infty, \\
\|\boldsymbol{\psi}\| &:= \max_{i=1,\dots,n} |\psi_i|.
\end{aligned}$$

Regarding the concatenation of the restriction and extension operator, we obtain the following two properties:

$$\begin{aligned}
&R \circ E_0 = \mathbf{I}, \\
&\|(E_0 \circ R)[\varphi] - \varphi\|_\infty \leq h \|\varphi'\|_\infty \quad \forall \varphi \in \mathcal{C}^1[0, 1],
\end{aligned}$$

where $\mathbf{I}$ is the identity matrix in $\mathbb{R}^{n \times n}$.

Integrals will be evaluated numerically by applying the mid-point rule. According to [22, p. 171], the error estimate

$$\int_a^b f(x)\, \mathrm{d}x = f\left(\frac{a+b}{2} \right)(b-a) + \frac{(b-a)^3}{24} f''(\xi) \tag{4}$$

holds for functions $f \in \mathcal{C}^2[a, b]$ and some intermediate point $\xi \in [a, b]$.

In subsequent sections, we will discuss two different discretizations of the integral operator S. Both discretizations are based on a piecewise constant approximation to the function φ. Since we choose our collocation points $\chi \in \mathcal{X}$ to be the mid-points of the grid cells Z, it is quite natural to approximate the integral by the mid-point rule. This approach yields the approximation S_0:

$$S_0 := E_0 \mathbf{S_0} R, \quad \text{where} \quad (\mathbf{S_0}\boldsymbol{\psi})_j := \sum_{i \neq j} \frac{\psi_i - \psi_j}{|\chi_i - \chi_j|} h. \tag{5}$$

Substituting the piecewise constant extension of a grid function in the integral operator S yields the alternative approximation $\tilde{S}_0$:

$$\tilde{S}_0 := SE_0R, \quad \tilde{\mathbf{S}}_\mathbf{0} = RSE_0 \quad \text{and} \quad (\tilde{\mathbf{S}}_\mathbf{0}\boldsymbol{\psi})_j := \sum_{i\neq j}(\psi_i - \psi_j)\left|\log\frac{s_i - \chi_j}{s_{i-1} - \chi_j}\right|. \tag{6}$$

In contrast to the operator S_0 that uses the mid-point rule for the integration, the operator $\tilde{S}_0$ performs an exact integration.

The multiplication operator C is approximated by

$$\mathbf{C}_{i,j} := C(\chi_i)\delta_{i,j}. \tag{7}$$

3.2. Approximation errors of the collocation schemes

Using the approximation (5) based on mid-point integration, one obtains for sufficiently smooth functions second-order accuracy in the collocation points $\chi \in \mathcal{X}$:

$$e_n := \|(R \circ S)[\varphi] - \mathbf{S}_\mathbf{0}(R\varphi)\| \leq Kh^2, \tag{8}$$

with a constant $K \leq \|\varphi'''\|_\infty/72 + \|\varphi''\|_\infty/8$. The proof of Equation (8) can be found in Appendix B.

Now the question arises, as to whether this second-order method is *super-convergent* in the collocation points or uniform. The term 'super-convergent' expresses the property, that collocation methods can yield a higher approximation and convergence order in the collocation points than on the rest of the interval [23, pp. 133–134]. Assume that $s \in Z_j$ for $j \in \{1, \ldots, n\}$. Following the proof of (8), we split the integral into its different parts. For the integral over Z_j, we obtain

$$\begin{aligned}\int_{s_{j-1}}^{s_j} \Phi_s(t)\,\mathrm{d}t &= \varphi'(s)(s_j + s_{j-1} - 2s) + \varphi''(\xi_{s,-})\frac{(s - s_{j-1})^2}{4} + \varphi''(\xi_{s,+})\frac{(s - s_j)^2}{4}\\ &\leq K\|\varphi'\|_\infty h.\end{aligned}$$

This already gives a hint on the super-convergence of the piecewise constant approximation for cell-centered collocation. A detailed analysis, similar to the proof of (8) shows

$$\|S[\varphi] - S_0[\varphi]\|_\infty \leq Kh \tag{9}$$

for some $K > 0$.

Concerning the alternative approximation $\tilde{S}_0$ involving analytic calculation of the integrals, one might expect a better approximation, since the integration is performed exact rather than applying the mid-point rule. Surprisingly, this is not the case, and we find :

$$\tilde{e}_n := \left\|(R \circ S)[\varphi] - \tilde{\mathbf{S}}_\mathbf{0}(R\varphi)\right\| \leq Kh\log\frac{1}{h}, \tag{10}$$

where $K > 0$ is some constant. The derivation of (10) is deferred to Appendix C.

Similar to (9), one can show that the operator $\tilde{S}_0$ approximates the operator S up to first order over the whole interval [0,1].

Table 1 shows results for the approximations $\mathbf{S}_\mathbf{0}$ and $\tilde{\mathbf{S}}_\mathbf{0}$ using as test cases

$$S[\varphi](s) = -L_n s^n + \sum_{k=0}^{n-1}\frac{1}{n-k}s^k \quad \text{for} \quad \varphi(s) = s^n, \tag{11}$$

Table 1. Absolute error and convergence rates in the collocation points for the test cases (11) using the approximations $\mathbf{S_0}$ (5) and $\tilde{\mathbf{S}}_\mathbf{0}$ (6)

	Approximation $\mathbf{S_0}$			
$\varphi(s)$	$n = 50$	$n = 100$	$n = 200$	γ
s^3	$2{\cdot}64 \times 10^{-4}$	$6{\cdot}64 \times 10^{-5}$	$1{\cdot}66 \times 10^{-5}$	2·00
s^2	$1{\cdot}00 \times 10^{-4}$	$2{\cdot}50 \times 10^{-5}$	$6{\cdot}25 \times 10^{-5}$	2·00
s^1	$1{\cdot}53 \times 10^{-15}$	$3{\cdot}33 \times 10^{-15}$	$5{\cdot}11 \times 10^{-15}$	
1	$3{\cdot}48 \times 10^{-15}$	$7{\cdot}91 \times 10^{-15}$	$1{\cdot}14 \times 10^{-14}$	

	Approximation $\tilde{\mathbf{S}}_\mathbf{0}$			
$\varphi(s)$	$n = 50$	$n = 100$	$n = 200$	γ
s^3	$8{\cdot}76 \times 10^{-3}$	$4{\cdot}47 \times 10^{-3}$	$2{\cdot}26 \times 10^{-3}$	0·98
s^2	$5{\cdot}96 \times 10^{-3}$	$3{\cdot}02 \times 10^{-3}$	$1{\cdot}52 \times 10^{-3}$	0·99
s^1	$3{\cdot}03 \times 10^{-3}$	$1{\cdot}53 \times 10^{-3}$	$7{\cdot}63 \times 10^{-4}$	1·00
1	$1{\cdot}37 \times 10^{-15}$	$2{\cdot}04 \times 10^{-15}$	$2{\cdot}73 \times 10^{-15}$	

where $-L_n = -\sum_{k=1}^{n} 2/k$ for $n \in \mathbb{N}_0$ and $L_0 = 0$ are the eigenvalues of S (see Equation (3)). The errors e_n and $\tilde{e}_n$ are defined in Equations (8) and (10). The *numerical convergence orders* γ and $\tilde{\gamma}$ are defined as

$$\gamma_n := \log_2 \frac{e_{n/2}}{e_n}, \qquad \tilde{\gamma}_n := \log_2 \frac{\tilde{e}_{n/2}}{\tilde{e}_n},$$

where $\log_2$ denotes the base-2 logarithm with respect to base 2. The expected $\mathcal{O}(h^2)$-error in the collocation points for the mid-point rule (operator $\mathbf{S_0}$) is clearly visible, as is the almost linear convergence for the method involving exact calculation of the integrals (operator $\tilde{\mathbf{S}}_\mathbf{0}$). For $\varphi(s) = 1$ and $\varphi(s) = s$, the mid-point rule is exact up to machine precision, whereas the second method is exact only for the trivial constant case.

3.3. Spectral properties

The discrete spectrum and associated eigenfunctions of the continuous operator S are explicitly known. One of the major results of the present work is, that the mid-point discretization $\mathbf{S_0}$ recovers exactly the spectrum of the integral operator S. Namely, using n collocation points, we obtain

$$\sigma(\mathbf{S_0}) = \{-L_k, k = 0, \ldots, n-1\}, \tag{12}$$

i.e. the collocation matrix $\mathbf{S_0}$ reproduces *exactly* the first n eigenvalues of the integral operator S. This result is proved in Appendix D.

Figure 1 shows the spectra of the matrices $\mathbf{S_0}$, $\tilde{\mathbf{S}}_\mathbf{0}$ and also the spectrum computed using a collocation scheme based on quadratic splines. The second and third spectra are computed numerically for different discretizations yielding matrices of size $n \times n$, where $n \in \{50, 100, 200\}$. The differences in the spectra are significant and the variations are especially notable for the collocation based on spline-approximation.

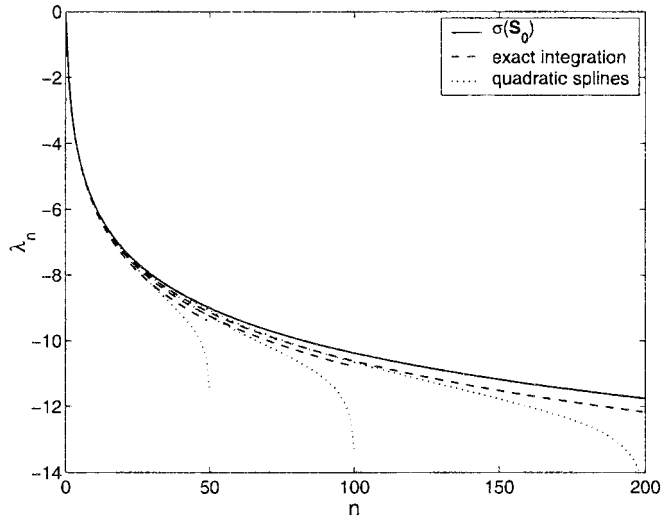

Figure 1. Spectra of the matrices $\mathbf{S_0}$ ('−'), $\tilde{\mathbf{S}}_\mathbf{0}$ ('- -') and of a matrix corresponding to a collocation scheme based on quadratic splines ('· · · ') are plotted.

Equation (12) is the discrete analogoue of a corresponding result for the continuous case and the proofs are similar, see [5,15]. The basis vectors $\boldsymbol{s^l}$ are *discrete monomials* and $\boldsymbol{p} \in$ span $\{\boldsymbol{s^l}, l = 0, \ldots, k$ for $k \leq n-1\}$ can be regarded as a *discrete polynomial of degree k*, if $\boldsymbol{ps^k} \neq 0$. In the derivation of (12) we find, that

$$\mathbf{S_0}[\text{span}\{\boldsymbol{s^l}, l = 0, \ldots, k\}] = \text{ span } \left\{\boldsymbol{s^l}, l = 0, \ldots, k\right\}$$

for all $k \leq n-1$. Hence, the matrix $\mathbf{S_0}$ maps discrete polynomials of degree k onto discrete polynomials of degree k.

From the theoretical investigation of S performed in [5,15], we know that eigenfunctions $\tilde{P}_k \in \mathcal{P}_k$ exist such that $S[\tilde{P}_k] = -L_k \tilde{P}_k$ and $\tilde{P}_k = s^k + \sum_{j=0}^{k-1} w_{k-1}^j \tilde{P}_j$. Thus, S diagonalizes the basis of the polynomial eigenfunctions $\tilde{P}_k$. Furthermore, $S[s^k] = -L_k s^k + q_{k-1}(s)$ where $q_{k-1} \in \mathcal{P}_{k-1}$.

Using Gram-Schmidt orthogonalization, we can construct a basis $\{\boldsymbol{u_0}, \ldots, \boldsymbol{u_{n-1}}\}$ of eigenvectors that diagonalizes $\mathbf{S_0}$ out of the discrete monomials used in (12). Now, the question arises, as to whether the *numerical* eigenvectors $\boldsymbol{u}_k$ of $\mathbf{S_0}$ converge for fixed k and $h \to 0$ to the eigenfunctions $\tilde{P}_k$ of the operator S.

The following estimate proved in Appendix E yields an affirmative answer : Let $k \in \mathbb{N}_0$ and $n > k$. Then

$$\left\| \boldsymbol{u_k} - R[\tilde{P}_k] \right\| \leq \frac{k(k-1)}{8} \left(1 + \frac{k-2}{9}\right) h^2 \sum_{j=0}^{k-1} \frac{1}{L_k - L_j}. \tag{13}$$

In summary, we have found that the numerical discretization $\mathbf{S_0}$ exactly reproduces the spectrum of the continuous operator and the eigenvectors of the numerical scheme converge to the eigenfunctions of the continuous operator.

3.4. Convergence of the collocation scheme

Next, we exploit the spectral properties of $\mathbf{S_0}$ and S to derive convergence results for the numerical scheme. The continuous equation

$$(C + S)[\varphi] = f, \quad \text{where} \quad S[\varphi](s) = \int_0^1 \frac{\varphi(t) - \varphi(s)}{|t - s|} \mathrm{d}t, \tag{14}$$

is replaced by its discrete counterpart

$$(\mathbf{C} + \mathbf{S_0})\boldsymbol{\psi} = \boldsymbol{f}, \tag{15}$$

where $\boldsymbol{f} = R[f]$ is the grid function associated to f. In a collocation point $\chi_i \in \mathcal{X}$, we obtain

$$(C + S)[\varphi](\chi_i) = \sum_{j=1}^{n} (\mathbf{C} + \mathbf{S_0})_{i,j} \boldsymbol{\psi}_j.$$

Since C is a multiplication operator according to Equation (7), the matrix $\mathbf{C}$ is diagonal. Hence $C[\varphi](\chi_i) = C(\chi_i)\varphi(\chi_i) = \sum_{j=1}^{n} \mathbf{C}_{i,j}(R\varphi)_j$. Introducing the error $\boldsymbol{e} = R[\varphi] - \boldsymbol{\psi}$ and the matrix $\mathbf{M} = \mathbf{C} + \mathbf{S_0}$, we obtain

$$\sum_j \mathbf{M}_{i,j} \boldsymbol{e}_j = \mathbf{S_0}(R[\varphi]) - (R \circ S)[\varphi].$$

In the case of $C = c = \text{const.}$ and $c \neq L_k$ for $k \in \mathbb{N}$, the eigenvalues of $\mathbf{M}$ are given by $\{c - L_k : k = 0, \ldots, n-1\}$. In particular, the matrix $\mathbf{M}$ is invertible and

$$\boldsymbol{e}_i = \sum_j \mathbf{M}^{-1}_{i,j} (\mathbf{S_0}(R[\varphi]) - (R \circ S)[\varphi])_j.$$

Thus, we obtain the estimate

$$\|\boldsymbol{e}\| \leq \left\|\mathbf{M}^{-1}\right\|_\infty \cdot \|(R \circ S)[\varphi] - \mathbf{S_0}(R[\varphi])\|.$$

The second factor is equal to the approximation error of the collocation scheme and is bounded by Kh^2 for some $K > 0$ due to Equation (8). Considering the first factor, let $\rho(\mathbf{M})$ denote the spectral radius and $\lambda_{\min}(\mathbf{M})$ be the eigenvalue of $\mathbf{M}$ with minimal absolute value. We have $\|\mathbf{M}\|_\infty \leq \sqrt{n}\rho(\mathbf{M})$. For $\|\mathbf{M}^{-1}\|_\infty$, we obtain

$$\|\mathbf{M}^{-1}\|_\infty \leq \sqrt{n}\rho(\mathbf{M}^{-1}) \leq \sqrt{n}\lambda_{\min}(\mathbf{M})^{-1}.$$

Since $C = c = \text{const.}$, the smallest eigenvalue of $\mathbf{M}$ is given by

$$\lambda_{\min}(\mathbf{M}) = \min_{\lambda \in \sigma(\mathbf{S_0})} |c + \lambda|.$$

For n large enough, *i.e.* for $c - L_n < 0$, this term is independent of n and bounded by some constant $K > 0$. Summarizing the results, we obtain

$$\|\boldsymbol{e}\| \leq K\sqrt{n}h^2 = Kh^{3/2},$$

which indicates a convergence late of at least 3/2 for the collocation method. The numerical results given in Table 2 exhibit a convergence rate of approximately 2. Whether this is a super-convergence or the estimates can be sharpened can be investigated by finding direct bounds for $\|\mathbf{M}\|_\infty$ without using the spectral norm as in the present approach.

If $c = L_k$ for some $k \in \mathbb{N}$, it is shown in [5] that there exist data f for which (14) has no solution. This occurs when $c = L_k$ for some $k \in \mathbb{N}$, whereupon the matrix $\mathbf{M}$ is singular.

Next we consider the case $C \neq$ const.. Until now, we used $C(s) = C =$ const. to derive lower bounds for the eigenvalues of $\mathbf{M}$. In the case of non-constant C and $\frac{1}{n}\sum_{i=0}^{n-l}(\boldsymbol{R}C)_i \neq L_k$ for $k \in \mathbb{N}$, we apply a perturbation argument, and apply the result for $C =$ const.

We recall a result due to [22, p. 63] : Let $\mathbf{A} \in \mathbb{R}^{n\times n}$ be regular and $\mathbf{E} \in \mathbb{R}^{n\times n}$ be a perturbation, such that $\|\mathbf{A^{-1}}\|\cdot\|\mathbf{E}\| \leq 1$ Then $\mathbf{A}+\mathbf{E}$ is regular and the estimate

$$\|(\mathbf{A}+\mathbf{E})^{-1}\| \leq \frac{\|\mathbf{A^{-1}}\|}{1-\|\mathbf{A^{-1}}\|\cdot\|\mathbf{E}\|}.$$

holds in any matrix-norm $\|\cdot\|$.

If $C \neq$ const., we define $c = \frac{1}{n}\sum_{i-0}^{n-1}(\boldsymbol{R}C)_i$, $\boldsymbol{\Delta = C - cI}$, $\mathbf{M} = \mathbf{C} + \mathbf{S_0}$ and $\hat{\mathbf{M}} = c\mathbf{I} + \mathbf{S_0}$ and apply the above result to the matrix $\mathbf{M} = \boldsymbol{\Delta} + \hat{\mathbf{M}}$, now viewed as a perturbation $\boldsymbol{\Delta}$ applied to the matrix $\hat{\mathbf{M}}$.

If $\|\hat{\mathbf{M}}^{-1}\|\cdot\|\boldsymbol{\Delta}\| \leq 1$, then

$$\|\mathbf{M^{-1}}\| \leq \frac{\|\hat{\mathbf{M}}^{-1}\|}{1-\|\hat{\mathbf{M}}^{-1}\|\cdot\|\boldsymbol{\Delta}\|}.$$

In particular

$$\|\mathbf{M}^{-1}\|_\infty \leq \frac{\sqrt{n}}{\lambda_{\min}(\hat{\mathbf{M}}) - \max\limits_{i=0,\ldots,n-1}|C_i - c|)}. \tag{16}$$

Equation (16) is restricted to the case

$$\max_{i=0,\ldots,n-1}|C_i - c| \leq \lambda_{\min}(\hat{\mathbf{M}}) = \min_{k\in\mathbb{N}_0}|c - L_{k-1}|.$$

For example, if $c = 5$, then $\min_{k\in\mathbb{N}_0}|c - L_{k-1}| = 0{\cdot}1$, whereas for $c = 14$, $\min_{k\in\mathbb{N}_0}|c - L_{k-1}| \approx 6{\cdot}986 \times 10^{-4}$ for $k = 615$.

4. Numerical treatment of the general Equation (1)

The discussion up to now has been concerned with a straight fiber exposed to normal or tangential flow, corresponding to Equation (2). In this section, we briefly discuss the numerical treatment of the more general Equation (1) rewritten as

$$\begin{aligned}\boldsymbol{f}(s) = {} & (C_1(s)\mathbf{I} + C_2(s)\boldsymbol{e_t}\boldsymbol{e_t'})\boldsymbol{\varphi}(s) \\ & \int_0^1 \left[\frac{\boldsymbol{\varphi}(t)}{R_0} - \frac{\boldsymbol{\varphi}(s)}{|s-t|} + \frac{\mathbf{M_0}\boldsymbol{\varphi}(t)}{R_0^3} - \frac{\boldsymbol{e_t}\boldsymbol{e_t'}\boldsymbol{\varphi}(s)}{|s-t|}\right]\mathrm{d}t.\end{aligned} \tag{17}$$

First, we note, that for a $\mathcal{C}^2$-centerline $\boldsymbol{x}_0$,

$$R_0 = \|\boldsymbol{x_0}(s) - \boldsymbol{x_0}(t)\| = |s-t| + \frac{\kappa}{2}|s-t|^2 + \mathcal{O}(|s-t|^3)$$

and

$$\frac{\mathbf{M_0}}{R_0^2} = \left(\frac{\boldsymbol{R_0}}{R_0}\right)\left(\frac{\boldsymbol{R_0}}{R_0}\right)' = \boldsymbol{e_t e_t'} + \frac{\kappa}{2}|s-t|(\boldsymbol{e_t e_n'} + \boldsymbol{e_n e_t'} + \mathcal{O}(|s-t|^2),$$

for $t \to s$, where κ is the curvature of the centerline. The integral in (17) exists for α-Hölder-continuous functions $\boldsymbol{\varphi} \in \mathcal{C}^{0,\alpha}[0, 1]$ and $\alpha \in (0,1]$. That is, for $t \to s$, the integrand of (17) 'reduces' to that of (14). For t away from s, the integrand of (17) expresses the effect of the curvature of the fiber's centerline. If the centerline does not self-intersect, *i.e.* if $\|\boldsymbol{x_0}(t) - \boldsymbol{x_0}(s)\| \geq K|s-t|$, then the terms containing R_0^{-1} and R_0^{-3} in (17) cannot have singularities for $t \neq s$.

As already stated, an explicit spectral theory for (17) is presently not available. Nevertheless, since the collocation method using piecewise constant *ansatz* functions and mid-point integration works well in the case of (2), a similar method can be used for solving (17).

Writing the components of (17) with respect to the global coordinate system in $\mathbb{R}^3$, we obtain a system of three coupled integral equations for the components $(\varphi_1, \varphi_2, \varphi_3) = \boldsymbol{\varphi}$. Using a piecewise constant ansatz for each component and discretizing the integrals with the mid-point quadrature formula, we obtain after some calculations a linear system $(\mathbf{C} + \mathbf{S_0}^{\text{full}})\boldsymbol{\varphi} = \boldsymbol{f}$,

$$\begin{pmatrix} \mathbf{S_0^{11}} & \mathbf{S_0^{12}} & \mathbf{S_0^{13}} \\ \mathbf{S_0^{21}} & \mathbf{S_0^{22}} & \mathbf{S_0^{23}} \\ \mathbf{S_0^{31}} & \mathbf{S_0^{32}} & \mathbf{S_0^{33}} \end{pmatrix} \begin{pmatrix} \varphi_1 \\ \varphi_2 \\ \varphi_3 \end{pmatrix} = \begin{pmatrix} f_1 \\ f_2 \\ f_3 \end{pmatrix},$$

for the components of $\boldsymbol{\varphi}$.

In the case of (2) (*e.g.* the fiber is aligned to the z-axis and $\boldsymbol{f} = (f_1, 0, 0)$), the off-diagonal blocks $\mathbf{S_0^{12}}, \mathbf{S_0^{13}}, \mathbf{S_0^{21}}, \mathbf{S_0^{23}}, \mathbf{S_0^{31}}, \mathbf{S_0^{32}}$ of the matrix $\mathbf{C} + \mathbf{S_0}^{\text{full}}$ drop out, and we obtain the familiar discretization $(c\mathbf{I} + \mathbf{S_0})\varphi_1 = f_1$, yielding the only force component in x-direction.

Normally, the matrix $\mathbf{C} + \mathbf{S_0}^{\text{full}}$ is a *full* and *non-symmetric* matrix with dimensions $(3n) \times (3n)$. If the fiber lies in a plane, *i.e.* if the torsion of the centerline vanishes, and if also the right hand side $\boldsymbol{f}$ has only components in this plane, then the local coordinate system spanned by the tangent $\boldsymbol{e_t}$ and the normal $\boldsymbol{e_n}$ of the fiber shall be used. In this situation, the binormal vector $\boldsymbol{e_b}$ is constant along the fiber. Using the decomposition of $\boldsymbol{\varphi}$ and $\boldsymbol{f}$ in the tangential and normal directions, we obtain a reduced system with dimensions $(2n) \times (2n)$.

5. Numerical results

The proposed collocation method is applied to different test cases. The solution of Equation (2), where the solution can be computed analytically using spectral methods is considered in Section 5.1. Section 5.2 shows a comparison with the analytic solution for flow past slender prolate spheroids, and Section 5.3 presents an example available from the literature requiring the numerical solution of the general equation (1).

5.1. Comparison with spectral methods

First, we compare the collocation method with a spectral method proposed in [15]. This method is based on an expansion of the right hand side f in terms of Legendre polynomials and exploits the explicit knowledge of the spectral properties of the integral operator S. The right-hand sides of Equations (2) are given by

Table 2. $\mathcal{L}^\infty$-error e_∞, the convergence order γ, and $\mathcal{L}^2$-error e_2 for $f(s)$ and $h_{1/5}(s)$

n	Test case f			Test case $h_{1/5}$		
	e_∞	γ	e_2	e_∞	γ	e_2
50	$1{\cdot}3225 \times 10^{-2}$		$1{\cdot}8765 \times 10^{-3}$	$2{\cdot}9890 \times 10^{-2}$		$9{\cdot}8854 \times 10^{-4}$
100	$3{\cdot}6285 \times 10^{-3}$	1·87	$4{\cdot}6120 \times 10^{-4}$	$8{\cdot}5338 \times 10^{-3}$	1·81	$2{\cdot}3864 \times 10^{-4}$
200	$9{\cdot}5020 \times 10^{-4}$	1·93	$1{\cdot}0672 \times 10^{-4}$	$2{\cdot}2858 \times 10^{-3}$	1·90	$5{\cdot}1680 \times 10^{-5}$
400	$2{\cdot}4409 \times 10^{-4}$	1·96	$1{\cdot}8061 \times 10^{-5}$	$5{\cdot}9209 \times 10^{-4}$	1·95	$4{\cdot}9725 \times 10^{-6}$

Table 3. $\mathcal{L}^\infty$-error $\tilde{e}_\infty$ along with the convergence order $\tilde{\gamma}$ and $\mathcal{L}^2$-error $\tilde{e}_2$ for $f(s)$ and $h_{1/5}(s)$ using the alternative approximation $\tilde{S}_0$

n	Test case f			Test case $h_{1/5}$		
	$\tilde{e}_\infty$	$\tilde{\gamma}$	$\tilde{e}_2$	$\tilde{e}_\infty$	$\tilde{\gamma}$	$\tilde{e}_2$
50	$3{\cdot}1178 \times 10^{-2}$		$6{\cdot}7005 \times 10^{-3}$	$6{\cdot}9975 \times 10^{-2}$		$3{\cdot}4469 \times 10^{-2}$
100	$1{\cdot}9763 \times 10^{-2}$	0·65	$2{\cdot}0394 \times 10^{-3}$	$4{\cdot}3879 \times 10^{-3}$	0·67	$1{\cdot}8684 \times 10^{-2}$
200	$1{\cdot}1858 \times 10^{-2}$	0·74	$6{\cdot}0923 \times 10^{-4}$	$2{\cdot}5837 \times 10^{-2}$	0·76	$7{\cdot}5078 \times 10^{-3}$
400	$5{\cdot}4897 \times 10^{-3}$	1·11	$1{\cdot}8528 \times 10^{-4}$	$1{\cdot}1865 \times 10^{-2}$	1·12	$2{\cdot}5611 \times 10^{-2}$

$$f(s) := -\sin(2\pi s),$$
$$h_\delta(s) := \frac{1}{\pi}\arctan\left(\frac{2s-1}{\delta}\right) + \frac{1}{2}.$$

The Legendre coefficients of the reference solution are obtained by use of `MAPLE V Release 4`. The expansion in the Legendre polynomial basis is cut off with a $\mathcal{L}^2$-error less than 10^{-5}. For the function $f(s) = -\sin(2\pi s)$, the first 11 coefficients guarantee a $\mathcal{L}^2$-approximation with an error of approximately $8{\cdot}4 \times 10^{-6}$. For $h_\delta(s) = \frac{1}{\pi}\arctan\left(\frac{2s-1}{\delta}\right) + \frac{1}{2}$ and $\delta = 5$, the first 39 coefficients are needed and yield a $\mathcal{L}^2$-error of $7{\cdot}8 \times 10^{-6}$. For $c = 5$, the solution is computed with $\mathcal{L}^2$-error less than 10^{-5}.

The collocation method uses $n = 50$ to 400 collocation points, *i.e.* the mesh width ranges between $h = 0{\cdot}02$ and $0{\cdot}0025$. Computating the solution requires the inversion of a full symmetric matrix with dimensions $n \times n$.

Table 2 lists the errors of the numerical solution in the $\mathcal{L}^\infty$- and $\mathcal{L}^2$-norm, both normalized with the $\mathcal{L}^\infty$- respectively $\mathcal{L}^2$-norm of the reference solution. For the error e_∞, the numerical convergence order γ is also given. The results show nearly quadratic numerical convergence rates for the collocation scheme.

Table 3 shows the analogous results for the alternative approximation $\tilde{S}_0$ to the integral operator S.

5.2. Flow past prolate spheroids

Next, we consider Stokes flow past slender prolate spheroids. Chwang and Wu [13] apply the singularity method to derive the exact force density acting on a prolate spheroidal particle,

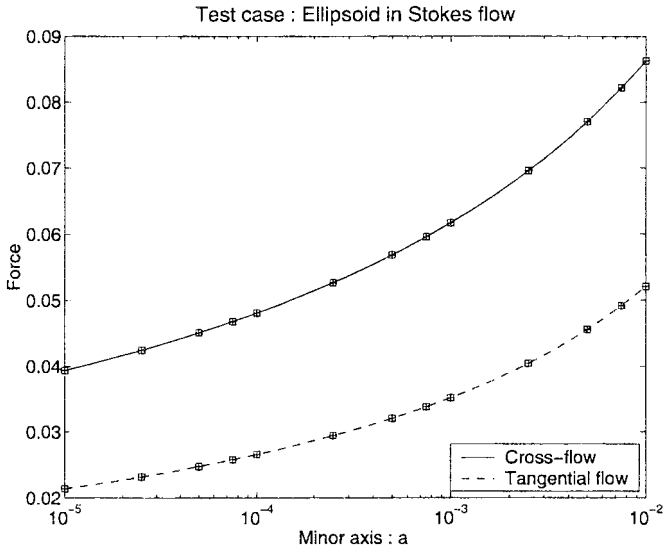

Figure 2. Force density φ for an prolate spheroid with minor to major half axes ratio a in Stokes flow. Analytical solution [13] ('–' and '- -'), and numerical solution of the integral equation ('⊞').

and show that the spatial distribution φ of Stokeslets is constant between the two foci of the spheroid and the normal component φ_z resp. the tangential component φ_x are given by

$$\varphi_z = u_{\infty,z}\frac{e^2}{-2e+(1+e^2)L_e}, \quad \varphi_x = u_{\infty,x}\frac{2e^2}{2e+(3e^2-1)L_e}, \tag{18a,b}$$

where $u_{\infty,z}$ is the normal free-stream velocity and $u_{\infty,x}$ is the tangential free-stream velocity. The eccentricity of the spheroid is $e = \sqrt{1-a^2}, a < 1$ is the minor semi-axis and $L_e = \log\frac{1+e}{1-e}$.

We compare this solution to the numerical solution obtained using our collocation method. The computations are carried out for ratio of minor to major half axes a ranging between 10^{-2} and 10^{-5} and the results are normalized with respect to the free-stream velocity $u_{\infty,x}$ respectively $u_{\infty,z}$. The numerical discretization uses $n = 100$ or 400 collocation points. The results for the two discretizations are nearly indistinguishable. The computed force distributions φ are constant up to machine precision along the centerline of the spheroid, in agreement with the exact solution.

Thanks to the hint of a referee, we remark, that for a constant free-stream velocity, the collocation scheme (15) reduces to $\boldsymbol{f} = \boldsymbol{u_0}$, where $\boldsymbol{u_0}$ is an eigenvector eigenvalue L_0.

Figure 2 shows the exact solution (solid line '–' for cross-flow and dashed line '- -' for tangential flow) and the numerical solution at discrete values for a (symbols '⊞'). The results are in very good agreement. In Figure 3, the difference between the exact and the numerical solution is plotted versus $\log a$. The error of the numerical solution is found to depend quadratically on the parameter a in the range $a = 10^{-2} \ldots 5 \times 10^{-5}$. This $(\mathcal{O})(a^2)$-difference can be explained by recalling that the approximations for the integral equation (1) was carried out up to terms of $\mathcal{O}(a)$. The different behavior of the error for smaller minor axes $a = 2{\cdot}5 \times 10^{-5} \ldots 10^{-5}$ is most likely due to round off errors in the computation of L_e. For $a = 10^{-5}$, the eccentricity e is equal to $\sqrt{1-10^{-10}}$, and $L_e = \log\frac{1+\sqrt{1-e^2}}{1-\sqrt{1-e^2}} \approx \log 3{\cdot}99 \times 10^{10}$.

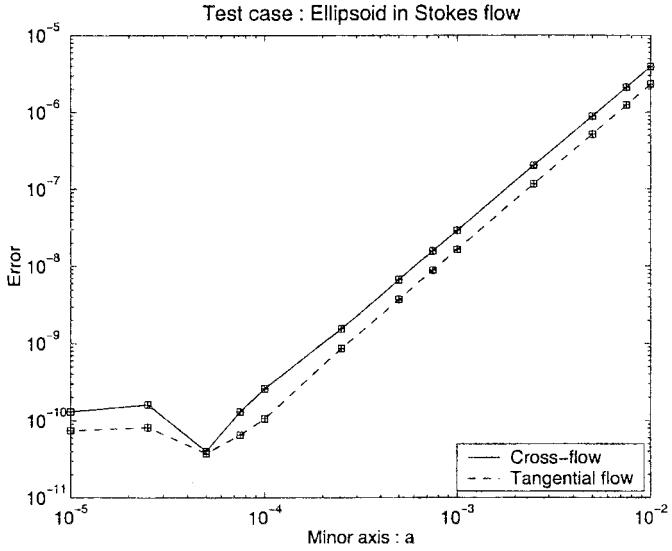

Figure 3. Differences between analytical solution and numerical solution for a prolate spheroid in Stokes flow.

Figure 4 presents a comparison between the exact solution and the numerical computation for different angles of attack. The *angle of attack* α is defined as the angle between the major semi-axis of the spheroid and the free-stream direction. The angle $\alpha = 0°$ corresponds to tangential flow, and the angle $\alpha = 90°$ corresponds to cross-flow. Intermediate cases require the numerical solution of (1) viewed as a coupled vector-integral equation for the two force components. The computations are done for minor to major axes ratio $a = 10^{-3}$ and 10^{-4}.

5.3. Circular arc in translational flow

Cox [24] considered the force exerted on a prolate spheroid with minor axis a, bent to a circular arc subtended between the angles θ_0 and θ_1. The free-stream velocity is $\boldsymbol{u}_\infty = \boldsymbol{e}_1$, as illustrated in Figure 5. Cox derived an expression for the force acting on the arc in the form of an expansion in terms of $1/\log a$. Johnson [18] derived an approximative solution obtained using an iteration procedure applied to an integral equation similar to (17).

For a discretization with $n = 400$ collocation points, minor to major axes ratio $a = 10^{-4}$ and angles $\theta_0 = 20°$ and $\theta_1 = 130°$, the resulting force based on Equation (17) was computed numerically using the collocation method and the results are shown in Figure 5. Good agreement is found with Johnson's approximation ('-.') and satisfactory agreement with Cox's ('--') asymptotic solution. The significant differences in Cox's approximation near the ends of the fiber are due to an inaccurate treatment of the fiber shape at the ends.

6. Conclusion and outlook

A collocation scheme for solving the Fredholm integral equations determining the forces density acting on a curved fiber with circular cross-section immersed in a Stokes-flow has been presented. Our analysis has shown that in the case of straight fibers, the collocation scheme based on the approximation (5) preserves the spectrum of the continuous integral operator. For slender prolate spheroids ($c = $ const.), the numerical solution converges quadratically with respect to the grid size to the analytic solution. In the general case of a curved fiber

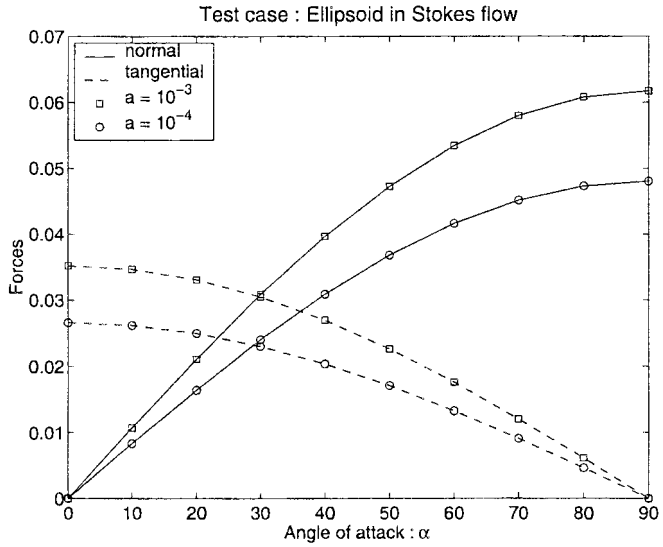

Figure 4. Forces for a prolate spheroid in Stokes flow and different angles of attack α. Exact solution ('$-$' and '--'), and numerical solution ('$\square$' and '$\circ$') for minor to major axes ratio $a = 10^{-3}$ and 10^{-4}.

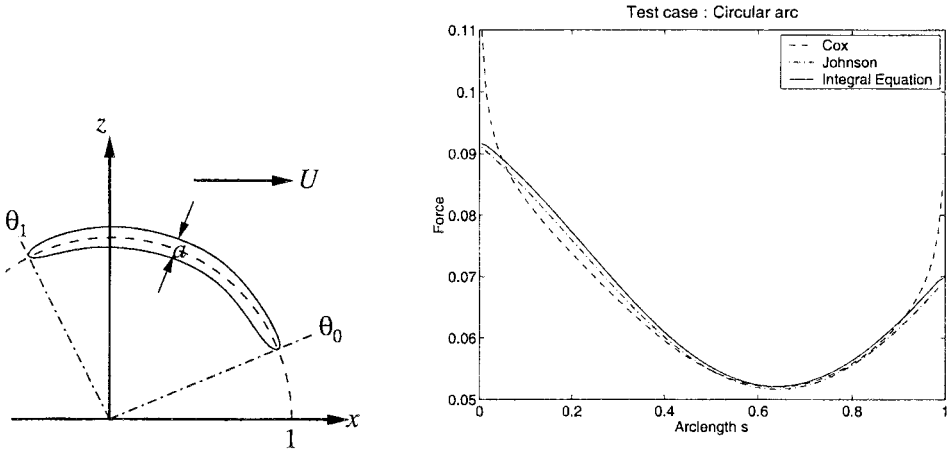

Figure 5. An ellipsoidal fiber shape with minor to major axes ratio a is bent to a planar circular arc subtended between θ_0 and θ_1. The right figure shows the force in x-direction for $\theta_0 = 20°$ and $\theta_1 = 130°$, including asymptotic results due to Cox [24] ('--'), Johnson [18] ('-.') and the numerical solution of the integral equation (17) ('$-$') for $a = 10^{-4}$.

where the spectrum is not explicitly known and hence convergence results are not available, the numerical solution shows good agreement with test cases available in the literature. In both cases, the numerical computations require solving a system of linear equations with a full and, in general, non-symmetric matrix. Advanced techniques involving approximating the system matrix by hierarchical $\mathcal{H}$-matrices [25,26] might be used to speed-up the calculations. An extension of the proposed collocation scheme to the integral equations in the case of Oseen flow is possible.

Appendix A. Derivation of Equation (1)

In this appendix we describe the main steps in the derivation of the integral equation (1) using slender-body approximation. For details, we refer to [5] or Keller and Rubinow [12].

Starting from the Stokes equations

$$\operatorname{div} \boldsymbol{u} = 0 \quad \text{and} \quad \mathbf{grad}\ p - \mu \Delta \boldsymbol{u} = \boldsymbol{f} \tag{A.1}$$

describing the linearized motion of a fluid in a domain Ω outside a fiber Ω_F, and using the no-slip boundary condition $\boldsymbol{u} = \boldsymbol{u_0}$ on the fiber surface, we make the following *ansatz* for the flow-field :

$$\boldsymbol{u}(\boldsymbol{x}) = \boldsymbol{u}_\infty(\boldsymbol{x}) + \int_0^L (\boldsymbol{\omega}(\boldsymbol{x} - \boldsymbol{x_0}(t); \nu)\boldsymbol{\varphi}(t) + \boldsymbol{\omega_2}(\boldsymbol{x} - \boldsymbol{x_0}(t); \nu)\beta(t))\, \mathrm{d}t, \tag{A.2}$$

where $\boldsymbol{u}_\infty$ is the free-flow velocity, L is the fiber centerline arc length, $\boldsymbol{\omega}(\boldsymbol{x} - \boldsymbol{x_0}(t); \nu)$ is the fundamental-solution (Stokeslet) of Stokes's equation, and $\boldsymbol{\omega_2}(\boldsymbol{x} - \boldsymbol{x_0}(t); \nu)$ is the Stokeslet doublet; $\boldsymbol{\varphi}$ and $\boldsymbol{\beta}$ are the distributions of the respective fundamental solutions. Explicitly

$$\boldsymbol{\omega}(\boldsymbol{x}; \nu) = \frac{1}{8\pi\nu}\left(\frac{\mathbf{I}}{R} + \frac{\boldsymbol{x}\boldsymbol{x'}}{R^3}\right),$$

where $R = \|\boldsymbol{x}\|_2$ and

$$\boldsymbol{\omega_2}(\boldsymbol{x}; \nu) = \frac{1}{8\pi\nu}\left(\frac{\mathbf{I}}{R^3} - 3\frac{\boldsymbol{x}\boldsymbol{x'}}{R^5}\right).$$

Physically, a Stokeslet corresponds to the flow field generated in whole $\mathbb{R}^3$ by a unit point force located at the origin.

We expand (A.2) asymptotically in the *'far field'* $|t - s| \gg a$ and in the *'near field'* $|t - s| = \mathcal{O}(a)$, and match the expansions, to derive the common part. A uniformly valid composite expansion is then obtained by adding the far field and the near field expansions and subtracting their common part. Now, the no-slip boundary condition can be applied to the composite expansion which is valid along the whole centerline of the fiber. The radial symmetry of the boundary condition around the circumference of the fiber allows us to obtain an expression for the distribution β of the doublets in terms of the distribution φ of the Stokeslets. The remaining integral equation (1) determines the distribution of the Stokeslets.

Appendix B. Proof of Equation (8)

Let $s, t \in [0,1]$, define $\Phi_s(t) = \frac{\varphi(t)-\varphi(s)}{|t-s|}$ with the convention $\Phi_s(s) = 0$, and let $j \in \{1, \ldots, n\}$. We split the integral in S into n parts over $[0, s_{j-1})$, $[s_{j-1}, s_j]$ and $(s_j, 1]$. Similarly, we split the sum into n parts for $i < j$ and $i > j$. For the second integral, we obtain the estimate

$$\begin{aligned}\int_{s_{j-1}}^{\chi_j} \Phi_{\chi_j}(t)\mathrm{d}t &= -\int_{s_{j-1}}^{\chi_j} \Phi'(\chi_j) + \frac{t - \chi_j}{2}\varphi''(\xi_{\chi_j,-})\mathrm{d}t \\ &= -\left[\frac{\varphi'(\chi_j)}{2}h - \frac{\varphi''(\xi_{\chi_j,-})}{16}h^2\right],\end{aligned}$$

with $\xi_{\chi_j,-} \in [s_{j-1}, \chi_j]$ and

$$\int_{\chi_j}^{s_j} \Phi_{\chi_j}(t)\mathrm{d}t = \left[\frac{\varphi'(\chi_j)}{2}h + \frac{\varphi''(\xi_{\chi_j,+})}{16}h^2\right]$$

with $\xi_{\chi_j,+} \in [\chi_j, s_j]$. Addition yields

$$\left|\int_{s_{j-1}}^{s_j} \Phi_{\chi_j}(t)\mathrm{d}t\right| = \left|\varphi''(\xi_{\chi,-}) + \varphi''(\xi_{\chi,+})\right| \frac{h^2}{16} \le \|\varphi''\|_\infty \frac{h^2}{8}.$$

For the first integral and the first summand, we obtain

$$\int_0^{s_{j-1}} \Phi_{\chi_j}(t)\mathrm{d}t - \sum_{i<j} \Phi_{\chi_j}(\chi_i) = \sum_{i<j} \Phi''_{\chi_j}(\xi_{\chi_j,i})\frac{h^2}{24}\left(\chi_j - \frac{h}{2}\right),$$

and for the last integral and last summand, we obtain

$$\int_{s_j}^1 \Phi_{\chi_j}(t)\mathrm{d}t - \sum_{i>j} \Phi_{\chi_j}(\chi_i) = \sum_{i>j} \Phi''_{\chi_j}(\xi_{\chi_j,i})\frac{h^2}{24}\left(1 - \chi_j - \frac{h}{2}\right),$$

Furthermore for $\xi < s$,

$$\begin{aligned}\Phi''_s(\xi) &= \frac{\varphi''(\xi)(s-\xi)^2 + 2(s-\xi)\varphi'(\xi) + 2(\varphi(\xi) - \varphi(s))}{(s-\xi)^3} \\ &= \frac{1}{(s-\xi)^3}\left[-\frac{(s-\xi)^3}{3}\varphi'''(\tilde{\xi})\right] = -\frac{\varphi'''(\tilde{\xi})}{3}\end{aligned}$$

with some $\tilde{\xi} \in (\xi, s)$. Similarly for $\xi > s$ and $\tilde{\xi} \in (s, \xi)$, we obtain $\Phi''_s(\xi) = \varphi'''(\tilde{\xi})/3$. Finally

$$\|(R \circ S)[\varphi] - \boldsymbol{S_0}(R\varphi)\| \le \left(\frac{\left\|\Phi''_{\chi_j}\right\|_\infty}{24} + \frac{\|\varphi''\|_\infty}{8}\right)h^2 \le \left(\frac{\|\varphi'''\|_\infty}{72} + \frac{\|\varphi''\|_\infty}{8}\right)h^2.$$

Appendix C. Proof of Equation (10)

Analogous to the proof of Equation (8), we fix a collocation point $\chi_j \in \mathcal{X}$ and split the integral into a part over Z_j and the remainder. For the integration over Z_j, we find

$$\left|\int_{Z_j} \Phi_{\chi_j}(t)\mathrm{d}t\right| \le \|\varphi''\|_\infty \frac{h^2}{8},$$

using the notations from the proof of Equation (8).

For the remaining integration, we use

$$|\varphi(t) - \varphi(\chi_i)| \le \|\varphi'\|_\infty \frac{h}{2},$$

where $t \in Z_i$, and obtain

$$\left|\sum_{i\neq j}\int_{Z_i} \frac{\varphi(t) - \varphi(\chi_i)}{|t - \chi_j|}\mathrm{d}t\right| \le \|\varphi'\|_\infty \frac{h}{2}\log\frac{\chi_j(1-\chi_j)}{h^2/4} \le \|\varphi'\|_\infty h \log\frac{1}{h},$$

which dominates the error (C.1).

Appendix D. Proof of Equation (12)

We need the preliminary result : Let $n, k \in \mathbb{N}_0$, then ,

$$\sum_{j=1}^{n}(2j-1)^k = \frac{2^k n^{k+1}}{k+1} - \sum_{\mu=1}^{k/2} C_{\mu,k} n^{k+1-2\mu},$$

where $\lfloor r \rfloor := \max_{n\in\mathbb{N}_0}\{n \le r\}$ denotes the Gauss-bracket,
$C_{\mu,k} = \frac{B_{2\mu}}{2\mu} 2^{k+1-2\mu}(2^{2\mu-1}-1)\binom{k}{2\mu-1}$ and B_n are the Bernoulli-numbers [27, Formula 0.122].

Now, let $\boldsymbol{s} = \left(\frac{i-1/2}{n}\right)_{i=1,\dots,n} \in \mathbb{R}^n$ and $\boldsymbol{s}^l = \left(s_i^l\right)_{i=1,\dots,n}$ for $l = 0, \dots, n-1$.

Then since the matrix with the columns $(\boldsymbol{s}^l)_{l=0,\dots,n-1}$ is a Vandermonde-matrix, $\{\boldsymbol{s}^0, \dots, \boldsymbol{s}^{n-1}\}$ is a basis of $\mathbb{R}^n$. Obviously, $\boldsymbol{s}^0 \in \ker \boldsymbol{S_0}$.

Next, we show that for $l \in \{1, \dots, n-1\}$ we have $\boldsymbol{S_0 s}^l = -L_l \boldsymbol{s}^l + \boldsymbol{p_{l-1}}$, where $\boldsymbol{p_{l-1}} \in \text{span}\,\{\boldsymbol{s}^0, \dots, \boldsymbol{s}^{l-1}\}$. Define $i' = i - 1/2$ and $j' = j - 1/2$. Then

$$\begin{aligned}
(\boldsymbol{S_0 s}^l)_i &= \frac{1}{n^l}\sum_{i\neq j}\frac{(j-\frac{1}{2})^l - (i-\frac{1}{2})^l}{|j-i|} \\
&= \frac{1}{n^l}\left(\sum_{j=1}^{n} + \delta_{i,j} - 2\sum_{j=1}^{i}\right)\left(\sum_{k=0}^{l-1} i'^{l-k-1} j'^k\right) \\
&= \frac{l(i')^{l-1}}{n^l} - \frac{2}{n^l 2^{l-1}}\sum_{k=0}^{l-1}(2i')^{l-k-1}\sum_{j=1}^{i}(2j-1)^k \\
&\quad + \frac{1}{n^l 2^{l-1}}\sum_{k=0}^{l-1}(2i')^{l-k-1}\sum_{j=1}^{n}(2j-1)^k \\
&= \frac{l(i')^{l-1}}{n^l} - \frac{2}{n^l 2^l}\sum_{k=0}^{l-1}(2i')^{l-k-1}\left(\frac{(2i)^{k+1}}{k+1} - \sum_{\mu} 2C_{\mu,k} i^{k+1-2\mu}\right) \\
&\quad + \frac{1}{n^l 2^l}\sum_{k=0}^{l-1}(2i')^{l-k-1}\left(\frac{(2n)^{k+1}}{k+1} - \sum_{\mu} 2C_{\mu,k} n^{k+1-2\mu}\right) \\
&= \frac{l(i')^{l-1}}{n^l} \underbrace{- \frac{2}{n^l 2^l}\left[(2i')\sum_{k=0}^{l-1}\frac{1}{k+1}\right.}_{(*)} - \sum_{k=0}^{l-1}(2i')^{l-k-1} \times . \\
&\quad \left. \times \left(\frac{1}{k+1}\sum_{m=1}^{k+1}\binom{k+1}{m}(-1)^m (2i)^{k+1-m} + \sum_{\mu} 2C_{\mu,k} i^{k+1-2\mu}\right)\right] \\
&\quad + \frac{1}{n^l 2^l}\sum_{k=0}^{l-1}(2i')^{l-k-1}\left(\frac{(2n)^{k+1}}{k+1} - \sum_{\mu} 2C_{\mu,k} n^{k+1-2\mu}\right) \\
&= -L_l \boldsymbol{s}^l + \boldsymbol{p_{l-1}}.
\end{aligned}$$

Note that the term $(*)$ is the only term that contains the vector $\boldsymbol{s}^l$. All the other terms are linear combinations of the vectors $\boldsymbol{s}^0, \ldots, \boldsymbol{s}^{l-1}$. Thus, writing $\mathbf{S_0}$ in the basis $\{\boldsymbol{s^k}\}_{k=0,\ldots,n-1}$, we obtain the following upper diagonal form

$$\mathbf{S_0} = \begin{bmatrix} 0 & * & \ldots & * \\ 0 & -L_1 & \ldots & * \\ \vdots & \vdots & \ddots & \vdots \\ 0 & 0 & \ldots & -L_{n-1} \end{bmatrix},$$

where the entries marked by $*$ correspond to the representation of $\boldsymbol{p_{l-1}}$ with respect to the basis $\{\boldsymbol{s^k}\}_{k=0,\ldots,n-1}$. The eigenvalues of this upper triangular matrix are the diagonal elements.

Appendix E. Proof of Equation (13)

The construction of a basis $(\boldsymbol{u_k})_{k=0,\ldots,n-1}$, in which $\mathbf{S_0}$ diagonalizes consists of the following two steps:

(1) Define $\boldsymbol{u_0} := \boldsymbol{s}^0$. Then $\mathbf{S_0}\boldsymbol{u_0} = -L_0\boldsymbol{u_0}$.
(2) Define $\boldsymbol{u_k} := \boldsymbol{s^k} + \sum_{j=0}^{k-1} r_{k-1}^j \boldsymbol{u_j}$, where $r_{k-1}^j = p_{k-1}^j/(L_k - L_j)$ and $\boldsymbol{p_{k-1}} = \sum_{j=0}^{k-1} p_{k-1}^j \boldsymbol{u_j}$.

Recalling Equation (12), *i.e.* $\mathbf{S_0}\boldsymbol{s^k} = -L_k\boldsymbol{s^k} + \boldsymbol{p_{k-1}}$ and using $(R \circ S)[s^k] = -L_k R[s^k] + R[q_{k-1}]$ from [5,15], we obtain

$$\|\boldsymbol{p_{k-1}} - R[q_{k-1}]\| \leq \|\mathbf{S_0}\boldsymbol{s^k} - (R \circ S)[s^k]\| \leq Kh^2 \tag{E.1}$$

using the estimate (8), where

$$K \leq \frac{\left\|(s^k)'''\right\|_\infty}{72} + \frac{\left\|(s^k)''\right\|_\infty}{8} \leq \frac{k(k-1)(k-2)}{72} + \frac{k(k-1)}{8}.$$

Due to the construction of the eigenvectors $\boldsymbol{u_k}$, i.e. $\boldsymbol{u_k} = \boldsymbol{s^k} + \sum_{j=0}^{l-1} r_{k-1}^j \boldsymbol{u_j}$ and $r_{k-1}^j = -\frac{p_{k-1}^j}{L_k - L_j}$ as well as $\boldsymbol{p_{k-1}} = \sum_{j=0}^{k-1} p_{k-1}^j \boldsymbol{u_j}$, we derive the estimate

$$\begin{aligned} \left\|\boldsymbol{u_k} - R[\tilde{P}_k]\right\| &\leq \sum_{j=0}^{k-1} \left\|r_{k-1}^j \boldsymbol{u_j} - w_{k-1}^j R[\tilde{P}_j]\right\| \leq \sum_{j=0}^{k-1} \frac{\left\|p_{k-1}^j \boldsymbol{u_j} - q_{k-1}^j R[\tilde{P}_j]\right\|}{L_k - L_j} \\ &\leq \sum_{j=0}^{k-1} \frac{\|\boldsymbol{p_{k-1}} - R[q_{k-1}]\|}{L_k - L_j}, \end{aligned}$$

and finally by (E.1)

$$\left\|\boldsymbol{u_k} - R[\tilde{P}_k]\right\| \leq \frac{k(k-1)}{8}\left(1 + \frac{k-2}{9}\right) h^2 \sum_{j=0}^{k-1} \frac{1}{L_k - L_j}.$$

References

1. H. Ockendon and E.L. Terril, A mathematical model for the wet-spinning process. *Euro. J. Appl. Math.* 4 (1993) 341–360.
2. A. Schöne, Modellbeschreibung des Fadenbildungsvorganges beim Schmelzspinnen unter den Bedingungen klassischer und hoher Spinngeschwindigkeiten. *Chemické vlákna* 32 (1982) 25–41.
3. H. Breuer, H. Haberkom, K. Hahn and P. Matthies, Schnellspinnen von Polyamid 6.6. *Chemiefasern/Textilindustrie* 42 (1992) 662–669.
4. R. Beyreuther, H. Brünig and D. Blechschmidt, High filament velocities in the underpressure spunbonding nonwoven process. *IFJ* (1997) 129–134.
5. T. Götz, *Interactions of Fibers and Flow : Asymptotics, Theory and Numerics*. Ph.D. thesis, University of Kaiserslautern, Germany (2000) 117 pp.
6. S.M. Dinh and R.C. Armstrong, A rheological equation of state for semiconcentrated fiber suspensions. *J. Rheology* 3 (1984) 207–227.
7. S.T. Chung and T.H. Kwon, Numerical simulation of fiber orientation in injection moulding of short-fiber-reinforced thermoplastics. *Polymer Eng. Sci.* 7 (1995) 604–618.
8. X. Fan, N. Phan-Thien and R. Zheng, A direct simulation of fibre suspensions. *J. Non-Newtonian Fluid Mech.* 74 (1998) 113–135.
9. M. Shelley and T. Ueda, The Stokesian hydrodynamics of flexing, stretching filaments. *Physica D* 146 (2000) 221–245.
10. C.S. Peskin and D.M. McQueen, A three-dimensional computational method for blood flow in the heart. I. Immersed elastic fibers in a viscous incompressible fluid. *J. Comp. Phys.* 81 (1989) 372–405.
11. J. Lighthill, *Mathematical Biofluiddynamics.* Philadelphia: SIAM (1975) 281 pp.
12. J.B. Keller and S.I. Rubinow, Slender-body theory for slow viscous flow. *J. Fluid Mech.* 75 (1976) 705–714.
13. A.T. Chwang and T.Y. Wu, Hydromechanics of low-Reynolds-number How. Part 2. Singularity methods for Stokes flow. *J. Fluid Mech.* 67 (1975) 787–815.
14. A. Sellier, Stokes flow past a slender particle. *Proc. R. Soc. London A.* 455 (1999) 2975–3002.
15. T. Götz and A. Unterreiter, Analysis and numerics of an integral equation model for slender bodies in low-Reynolds-number flows. *J. lntegral Equ. and Applics.* 12 (2000) 225–270.
16. H. Zhou and C. Pozrikidis, Adaptive singularity method for Stokes flow past particles. *J. Comp. Phys.* 117 (1995) 79–89.
17. R.A. Handelsman and J.B. Keller, Axially symmetric flow around a slender body. *J. Fluid Mech.* 28 (1967) 131–147.
18. R.E. Johnson, An improved slender-body theory for Stokes flow. *J. Fluid Mech.* 99 (1980) 411–431.
19. G.K. Batchelor, Slender-body theory for particles of arbitrary cross-section in Stokes flow. *J. Fluid Mech* 44 (1970) 419–440.
20. H. Power, Matched-asymptotic analysis of low-Reynolds number flow past a cylinder of arbitrary cross-sectional shape. *Math. Aplic. Comp.* 9 (1990) 111–122.
21. T. Kida and T. Take, Integral approach of asymptotic expansions for low-Reynolds-number flow past an arbitrary cylinder. *JSME Int. J., Series II* 35 (1992) 138–143.
22. R. Schaback and H. Werner, *Praktische Mathematik.* Berlin: Springer (1992), 326 pp.
23. W. Hackbusch, *Integralgleichungen : Theorie und Numerik.* Stuttgart: Teubner (1989) 374 pp.
24. R.G. Cox, The motion of long slender bodies in a viscous fluid. Part 1. General theory. *J. Fluid Mech.* 44 (1970) 791–810.
25. W. Hackbusch, A sparse matrix arithmetic based on H-matrices. Part I: Introduction to H-matrices. *Computing* 62 (1999) 89–108.
26. W. Hackbusch and B.N. Khoromskij, A sparse H-matrix arithmetic. Part II: Application to multi-dimensional problems. *Computing* 64 (2000) 21–47.
27. I.S. Gradshtyn and I.M. Rhyzik, *Table of Integrals, Series and Products.* New York: Academic Press (1973) 1086 pp.